PASJ: Publ. Astron. Soc. Japan **50**, 501–507 (1998)

Hydrogen Shell-Burning Models for RX J0925.7−4758

Reiun HOSHI
Department of Physics, Rikkyo University, Nishi-Ikebukuro, Tokyo 171-8501

(Received 1988 January 10; accepted 1988 August 10)

Abstract

We have constructed models of accreting white dwarfs in steady hydrogen burning for the supersoft X-ray source RX J0925.7−4758. A white dwarf with a mass of around $1.4\,M_\odot$ has been found to account for the blackbody temperature and the bolometric luminosity, determined from ASCA observations. Our models indicate that the color temperature is higher by up to 30% than the effective temperature. To be exact, the soft X-ray spectra differ considerably from the blackbody. The models discussed in this paper can also be applied to the other supersoft X-ray sources.

Key words: Accretion — Stars: individual (RX J0925.7−4758) — Stars: white dwarfs — X-rays: sources

1. Introduction

Dozens of Supersoft X-ray sources (SSS) have been discovered by the Einstein Observatory and ROSAT (for review refer Hasinger 1994; Rappaport, Di Stefano 1996; Cowley et al. 1996; Kahabka, Trümper 1996). Among these, the galactic SSS, RX J0925.7−4758, has a unique property in that X-rays are emitted above 0.5 keV. The solid-state spectrometers onboard the ASCA satellite have a superior energy resolution and X-ray sensitivity above 0.4 keV. Thus, RX J0925.7−4758 was a good target for ASCA to study more from its fine spectroscopic data. ASCA observations were conducted on 1994 December 22, for 20 ks. Although unacceptable (reduced $\chi^2 \sim 10$,) blackbody fits to the ASCA data give the temperature, $kT \sim 46$ eV; the hydrogen column density, $N_{\rm H} \sim 2 \times 10^{22}$ cm^{-2}; and the bolometric luminosity, $L_{\rm Bol} \sim 1.5 \times 10^{40} (d/1\ {\rm kpc})^2$ erg s^{-1} (Ebisawa et al. 1997), consistent with the ROSAT result (Motch et al. 1993). Noticeable absorption edges, however, were seen at around 0.7, 0.9, and 1.4 keV (Ebisawa et al. 1997). The best-fit blackbody parameters introducing absorption edges differ remarkably from those of the blackbody fits alone: $kT \sim 98$ eV, $N_{\rm H} \sim 0.9 \times 10^{22}$ cm^{-1}, and $L_{\rm Bol} \sim 1.6 \times 10^{35} (d/1\ {\rm kpc})^2$erg s^{-1} (Ebisawa et al. 1997; Asai et al. 1998). Assuming white dwarfs, hydrogen shell-burning models for SSS require a luminosity near to the Eddington limit (van den Heuvel et al. 1992). To apply these models, RX J0925.7−4758 will have a distance of >10 kpc. The high blackbody temperature determined from the ASCA data together with a luminosity close to the Eddington limit $\sim 10^{38}$erg s^{-1} yields a radius of 3000 km, which implies a white-dwarf mass of $\sim 1.3\,M_\odot$. This small radius led Ebisawa et al. (1997) to suggest the possibility of a massive white dwarf close to the Chandrasekhar limit for RX J0925.7−4758.

In this paper, we present hydrogen shell-burning models for RX J0925.7−4758. Similar calculations have been carried out by Fujimoto (1982a, 1982b); his results have been applied to recurrent SSS (Kahabka 1995). In our calculations, however, special emphasis is placed on the color temperature as a function of the mass of the white dwarf and the luminosity. Assuming a massive white dwarf, we construct hydrogen shell-burning models that account for the blackbody temperature and the luminosity determined from the ASCA observations. The model constructed in this paper can also be applied to those SSSs in which blackbody temperatures and the luminosities have been determined observationally. If the mass of RX J0925.7−4758 is assumed to be close to $1.3\,M_\odot$, in order to obtain the observed blackbody temperature $T_{\rm obs}$ the required source distance seems to be too distant. Contrarily, if the mass is assumed to be close to the Chandrasekhar limit, the luminosity is fairly smaller than the Eddington limit to obtain $T_{\rm obs}$. In a low-luminosity white dwarf, the hydrogen-burning shell would be unstable (Sienkiewicz 1980). A proper model can be constructed for a mass greater than $1.3\,M_\odot$. In order to determine the mass of the RX J0925.7−4768, stability analyses are essential, although such analyses are beyond the scope of the present paper. In this paper we relax the condition that the luminosity is close to the Eddington limit. This allows us a deep understanding of the characteristics of an accreting white dwarf undergoing steady hydrogen shell-burning.

2. Hydrogen Shell-Burning Model

2.1. Mass Radius Relation

In this paper we confine ourselves to a white dwarf of mass greater than $1.0\,M_\odot$. The radius R of a white dwarf of mass M can be approximated to be in the range from 1.0 to $1.45\,M_\odot$, as

$$R = R_0 \left(1 - \frac{M}{M_{\rm Ch}}\right)^{1/2}, \tag{1}$$

where $M_{\rm Ch}$ is the Chandrasekhar limiting mass ($= 1.46\,M_\odot$), and $R_0 = 1.0 \times 10^4$ km.

2.2. Eddington Temperature

If the luminosity of the accreting white dwarf is close to the Eddington limit $L_{\rm Edd}$, it is convenient to define the Eddington temperature $T_{\rm e,\,Edd}$ by

$$L_{\rm Edd} = 4\pi R^2 \sigma T_{\rm e,\,Edd}^4\,, \tag{2}$$

where σ is the Stefan–Boltzmann constant. Assuming the electron-scattering opacity $\kappa_{\rm e}$ to dominate the absorptive opacities, the Eddington temperature is given by

$$T_{\rm e,\,Edd} = \left(\frac{cGM_{\rm Ch}}{\kappa_{\rm e}\sigma {R_0}^2}\right)^{1/4} \left(\frac{M}{M_{\rm Ch}}\right)^{1/4} \left(1 - \frac{M}{M_{\rm Ch}}\right)^{-1/4}. \tag{3}$$

As the luminosity approaches the Eddington limit, the overlaid envelope on the hydrogen-burning shell is forced to swell abruptly. Thus, the radius R in equation (2) must be replaced by the radius to the surface of the expanded envelope. Equation (3) gives no proper measure of the effective temperature. If the luminosity is less than half of the Eddington limit, we have found that the thickness of the envelope can be practically ignored compared with the radius of the white dwarf. In this case, the effective temperature of a white dwarf of luminosity L is given approximately by

$$T_{\rm e} = T_{\rm e,\,Edd} \left(\frac{L}{L_{\rm Edd}}\right)^{1/4}. \tag{4}$$

If hydrogen burning supplies most of the radiative energy, the accretion rate is given, in terms of the available nuclear energy per unit mass $E_{\rm H}$ for $4{\rm H} \rightarrow {\rm He}$, by

$$\dot{M} = L\,/\,E_{\rm H}\,, \tag{5}$$

where $E_{\rm H} = 4.2 \times 10^{18}$ erg g^{-1} for the fraction of hydrogen by mass in the envelope, $X = 0.7$.

2.3. Plane-Parallel Approximation

In this subsection we formulate the analytical solutions of the hydrogen-rich envelope under the plane-parallel approximation. This approximation fails as L approaches $L_{\rm Edd}$. Analytical solutions applied to a wider range of L have been derived by Sugimoto and Fujimoto (1978), and Fujimoto (1982a, 1982b). We did not use their method, since the plane-parallel approximation is simple and provides analytical solutions applicable to moderate $L/L_{\rm Edd}$.

Provided that the thickness of the envelope h_0 is smaller than the radius of the white dwarf,

$$h_0 \ < \ R\,, \tag{6}$$

the plane-parallel approximation can be applied, which enables us to solve analytically the structure of the envelope under steady hydrogen burning at its base. The equation of hydrostatic balance in the radial direction may be solved, after replacing $R + h_0$ with R by

$$P_1 - P = \frac{GM}{R^2}\,m\,, \tag{7}$$

where the suffix 1 refers to the base of the envelope (the base of the hydrogen burning shell) and m is the column mass,

$$m = \int_0^h \rho\, dh\,. \tag{8}$$

Defining the total column mass from the base to the photosphere, m_0, the pressure at the base is given by

$$P_1 \ = \ \frac{GM}{R^2}\,m_0\,. \tag{9}$$

Approximating that the luminosity is constant throughout the whole envelope (this approximation is fulfilled when the column mass of the hydrogen burning shell is smaller than m_0), the equation for the radiative transport of energy can be solved as

$$T_1^4 \ - \ T^4 = \frac{3}{a}\left(\frac{L}{L_{\rm Edd}}\right)\frac{GM}{R^2}\,m\,, \tag{10}$$

since the opacity is dominated by electron scattering. Here, T is the temperature at the column mass m measured from the base of the envelope, and a is the radiation-density constant. From equation (10) the column mass m_0 may be written in terms of T_1, the temperature at the base of the envelope, as

$$m_0 \ = \ \frac{L_{\rm Edd}}{L}\left(\frac{GM}{R^2}\right)^{-1}\frac{aT_1^4}{3}\,. \tag{11}$$

Combining equations (9) and (11), together with the equation of state, the density at the base of the envelope is given by

$$\rho_1 \ = \ \frac{\mu m_{\rm H}}{k}\left(\frac{L_{\rm Edd}}{L} \ - \ 1\right)\frac{aT_1^3}{3}\,, \tag{12}$$

where $m_{\rm H}$ is the mass of the hydrogen atom and μ is the mean molecular weight, respectively. Also, from equations (9) and (11) we have

$$P_{\rm r,\,1} = \left(\frac{L}{L_{\rm Edd}}\right) P_1 \,, \tag{13}$$

where $P_{\rm r}$ is the radiation pressure which can be ignored if $L/L_{\rm Edd} \ll 1$. In the following equations, however, both the radiation and gas pressures are fully taken into account. From equations (10) and (11), T is simply written as

$$T = T_1 \left(1 - \frac{m}{m_0}\right)^{1/4} \,, \tag{14}$$

and from equations (7) and (9) the pressure is given by

$$P = P_1 \left(1 - \frac{m}{m_0}\right) \,. \tag{15}$$

The equation of state determines the density in a similar form,

$$\rho = \rho_1 \left(1 - \frac{m}{m_0}\right)^{3/4} \,. \tag{16}$$

It is noted that the gas and radiation pressures are both proportional to $(1 - m/m_0)$, the same dependence as the total pressure. The ratio of the gas to radiation pressure remains constant throughout the whole envelope.

One who wishes to utilize the independent variable h in place of m may solve the differential equation $dm/dh = \rho$ by substituting equation (16), as

$$\left(1 - \frac{m}{m_0}\right) = \left(1 - \frac{\rho_1 h}{4m_0}\right)^4 \,. \tag{17}$$

Putting $m = m_0$ in the above equation, we obtain the thickness of the envelope,

$$h_0 = \frac{4m_0}{\rho_1} \,. \tag{18}$$

One of the crucial constraints placed in solving the above equations is, therefore,

$$\frac{4m_0}{\rho_1} < R \,. \tag{19}$$

2.4. Structure of the Hydrogen-Burning Shell

The energy generation rate due to the CNO cycle is given by (Kippenhahn, Weigert 1990)

$$\varepsilon_{\rm CNO} = \varepsilon_0 \rho T_7^{-2/3} \exp(-70.68 T_7^{-1/3}) \ [\rm erg\ g^{-1}\ s^{-1}], \tag{20}$$

with $\varepsilon_0 = 2.6 \times 10^{25}$ erg cm^3 g^{-2} s^{-1} for an assumed fraction of $X = 0.7$ and $X_{\rm CNO} = 0.02$. Here, T_7 is the temperature in units of 10^7 K. Approximating $\varepsilon_{\rm CNO}$ by

$$\varepsilon_{\rm CNO} = \varepsilon_0^{(1)} \rho T^s \tag{21}$$

with

$$s = (70.68\, T_7^{-1/3} - 2)/3 \,, \tag{22}$$

the radiative flux per unit area is given by

$$l = \varepsilon_{\rm CNO,\,1}\, \delta\, m_0 \,, \tag{23}$$

where $\varepsilon_{\rm CNO,\,1}$ is the energy generation rate at the base of the hydrogen-burning shell and $\delta = 4/(7+s)$. The column mass of the nuclear-burning shell amounts to $\delta m_0 = [4/(7+s)]m_0 \sim 0.2 m_0$ around a temperature of 10^8 K. Thus, $L =$ constant throughout the whole envelope is a fairly good approximation.

Substituting equations (11) and (12), we have

$$l = A T_1^{19/3} \exp(-1.52 \times 10^4\, T_1^{-1/3}) \tag{24}$$

with

$$A = \varepsilon_0^{(2)} \frac{\mu m_{\rm H}}{k} \left(\frac{a}{3}\right)^2 \frac{R_0^2}{G M_{\rm Ch}} \frac{L_{\rm Edd}}{L} \left(\frac{L_{\rm Edd}}{L} - 1\right) \frac{M_{\rm Ch}}{M} \times \left(1 - \frac{M}{M_{\rm Ch}}\right) \delta \,, \tag{25}$$

where $\varepsilon_0^{(2)} = \varepsilon_0 \times 10^{14/3}$. On the other hand, the radiative flux l is simply written as

$$l = \frac{L}{4\pi R^2} = \frac{c G M_{\rm Ch}}{\kappa_{\rm e} R_0^2} \frac{L}{L_{\rm Edd}} \frac{M}{M_{\rm Ch}} \left(1 - \frac{M}{M_{\rm Ch}}\right)^{-1} \,. \tag{26}$$

Equating the above two equations for a given L or $L/L_{\rm Edd}$ and M, the temperature T_1 at the base of the burning-shell can be determined, from which the density ρ_1, the column mass m_0 and thickness of the envelope h_0 are determined, respectively.

Figure 1 shows the temperature and the density at the base of the hydrogen burning shell as a function of $L/L_{\rm Edd}$. Each curve is labeled according to the mass of the white dwarf.

3. Color Temperature

The observed blackbody temperature $T_{\rm obs}$ is well determined irrespective of the distance to the source. Hence, we place reliance on $T_{\rm obs}$ as a good parameter deduced from observations. A more critical argument will be given in section 4. The effective temperature $T_{\rm e}$ defined in equation (4) can be compared with $T_{\rm obs}$ if the absorptive opacity is comparable to, or dominated over, the electron-scattering opacity near to the photosphere. If the adjacent layers inside the photosphere are dominated by the electron-scattering opacity, it is absurd to argue based on the effective temperature. Most photons escape by random walking due to electron scattering out of the layers, $\tau_* [= \sqrt{\tau_{\rm a}(\tau_{\rm a} + \tau_{\rm s})}] < 1$, without being destroyed by true absorption, where $\tau_{\rm a}$ and $\tau_{\rm e}$ are the

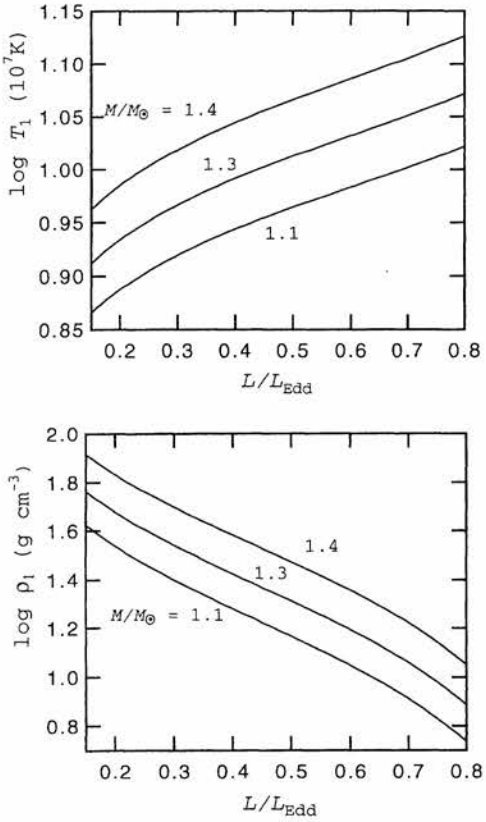

Fig. 1. Temperature and density at the base of the hydrogen-burning shell as a function of $L/L_{\rm Edd}$ for accreting white dwarfs with different mass.

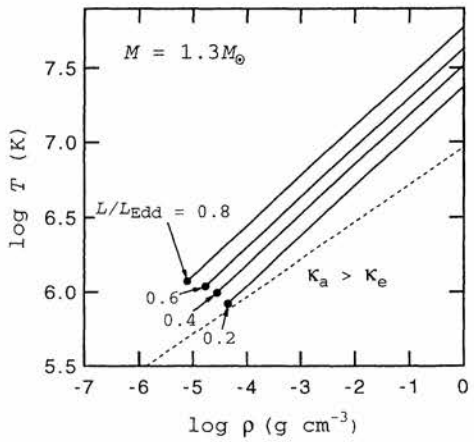

Fig. 2. Temperature as a function of the density in the envelope of a 1.3 $M_\odot$ white dwarf for different values of $L/L_{\rm Edd}$. The filled circles refer to the photosphere.

optical depths for the absorptive and electron-scattering opacity, respectively (Rybicki, Lightman 1979). Photons emitted at an optical depth of $\tau_* \sim 1$ are observed at a distant observer.

In figure 2 we plot the temperature T as a function of the density ρ in the envelope for a white dwarf with mass 1.3 $M_\odot$ for different values of $L/L_{\rm Edd}$. The filled circles refer to the photosphere, where the temperature is equal to $T_{\rm e}$ [see equation (4)]. The broken line shows the locus where the electron-scattering opacity $\kappa_{\rm e}$ is equal to the absorptive opacity $\kappa_{\rm a}$. The region to the left of this broken line is dominated by the electron scattering opacity. Figure 2 indicates that the effective temperature cannot be compared with $T_{\rm obs}$ for $L/L_{\rm Edd}$ larger than 0.2.

In order to determine the color temperature at $\tau_* \sim 1$, we adopt the gray-atmosphere approximation (Mihalas 1978). In the outer envelope it is convenient to use the column mass m' measured from the surface of the star, which can be given by $m' = m_0 - m$. The temperature and density can be written as

$$T = T_1 \left(\frac{m'}{m_0}\right)^{1/4}, \tag{27}$$

$$\rho = \rho_1 \left(\frac{m'}{m_0}\right)^{3/4} \tag{28}$$

in place of equations (14) and (16). However, since in the layers of $\tau_* < 1$, the photon flux is transmitted without loss of the energy, although individual photons are scattered many times, we approximate these layers with $\tau_* \leq 2/3$ to be isothermal with the temperature (T_*; the temperature at $\tau_* = 2/3$). Because the optical depth due to electron scattering $\tau_{\rm e}$ is larger than unity in the layers, we can take the radiation pressure into account, even if the layers are isothermal.

Under Eddington's approximation, the radiation pressure is given by (Mihalas 1978)

$$P_{\rm R} = \frac{L}{4\pi R^2 c}\left(\tau_{\rm e} + \frac{2}{3}\right). \tag{29}$$

In terms of equation (29) the density in the isothermal layers is given by

$$\rho = \frac{\mu m_{\rm H}}{kT_*}\left(1 - \frac{L}{L_{\rm Edd}}\right)\frac{GM}{R^2}m'. \tag{30}$$

To derive the above equation we have neglected the last term in equation (29).

The (Rosseland-mean) opacity table (WKM13; $X = 0.7, Y = 0.28, Z = 0.02$) of Weiss et al. (1990) can be approximated in the relevant ranges of temperatures and densities by

$$\kappa_{\rm a} = \kappa_0 \rho T^{-4} \quad [{\rm cm^2\,g^{-1}}], \tag{31}$$

with $\kappa_0 = 2.5 \times 10^{27}$ cm^5 g^{-2} K^4. Approximating $d\tau_* = \sqrt{\kappa_{\rm a}\kappa_{\rm e}}dm'$, we have

$$\tau_* = \frac{2}{3}\left[\kappa_0\kappa_e T_*^{-4}\left(\frac{\mu m_H}{kT_*}\right)\left(1-\frac{L}{L_{Edd}}\right)\frac{GM}{R^2}\right]^{1/2} m'^{3/2}, \quad (32)$$

Putting $\tau_* = 2/3$ and using equation (30) we have T_* as a function of ρ_*, the density at $\tau_* = 2/3$,

$$T_* = (\kappa_0\kappa_e)^{1/2}\frac{k}{\mu m_H}\left(1-\frac{L}{L_{Edd}}\right)^{-1}\frac{R}{GM}\rho_*^{3/2}. \quad (33)$$

These T_* and ρ_* must lie on the curve given by equations (27) and (28), which can be written as

$$T = \left[\frac{k}{\mu m_H}\left(\frac{L_{Edd}}{L}-1\right)^{-1}\frac{3}{a}\right]^{1/3}\rho^{1/3}. \quad (34)$$

Eliminating ρ_* from equations (33) and (34) in which we replace T and ρ with T_* and ρ_*, we have

$$T_* = (\kappa_0\kappa_e)^{-1/7}\left(\frac{k}{\mu m_H}\right)^{1/7}\left(\frac{L}{L_{Edd}}\right)^{3/7} \times\left(1-\frac{L}{L_{Edd}}\right)^{-1/7}\left(\frac{3}{a}\right)^{3/7}\left(\frac{GM}{R^2}\right)^{2/7}. \quad (35)$$

If we assume the layers with $\tau_* \leq 1$ to be isothermal, T_* differs from equation (35) by a factor of $(3/2)^{2/7}$. As for the radius R, we add the thickness of the envelope h_0 to the radius of the underlying white dwarf,

$$R = R_0\left(1+\frac{h_0}{R_0}\right)\left(1-\frac{M}{M_{Ch}}\right)^{1/2}. \quad (36)$$

It is noted that equation (35) involves no physical values at the bottom of the hydrogen burning shell, except for h_0 in equation (36).

We regard T_* as being determined from equation (35) as the color temperature $T_{color} = T_*$, which is to be compared with the observed blackbody temperature T_{obs}. It is noted that the color temperature [equation (35)] is valid for $T_{color} > T_e$ in our approximation, which has been taken into account in figure 3. Figure 3 shows the color temperature as a function of L/L_{Edd} for white dwarfs of masses 1.1 to 1.4 $M_\odot$. The broken curves show the effective temperature for 1.4 $M_\odot$ and 1.1 $M_\odot$, which has a plateau at around $L/L_{Edd} = 0.5$–0.6, depending on the mass of the white dwarf. The effective temperature is given by equations (4) and (2), where we have used equation (36). The thickness of the envelope h_0 grows steeply with L/L_{Edd}, so that the slope of the color temperature is decreased, since $T_{color} \propto R^{-4/7}$. At $L/L_{Edd} = 0.6$ the color temperature is larger by 25% and 35% (40% and 50% for $\tau_* = 1$) than the effective temperature for the white dwarfs of mass 1.4 $M_\odot$ and 1.1 $M_\odot$, respectively.

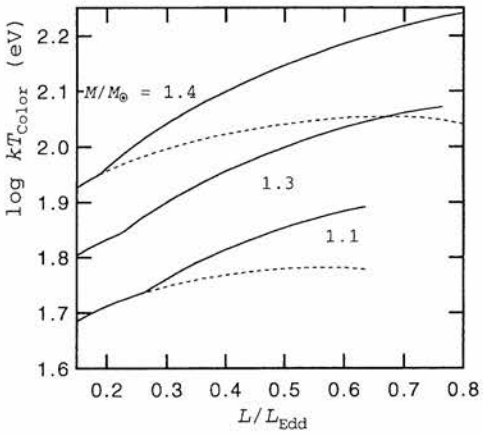

Fig. 3. Color temperature as a function of L/L_{Edd} for different values of the mass. The broken lines are the effective temperature for masses of 1.4 $M_\odot$ and 1.1 $M_\odot$, respectively.

4. Discussion

In order to account for the new properties of RX J0925.7−4758 obtained from the ASCA observations, we have constructed the structure of the envelope undergoing hydrogen burning at its base. Analytical calculations have been performed for luminosities smaller than $L/L_{Edd} < 0.5$ for 1.1 $M_\odot$, 0.6 for 1.3 $M_\odot$ and 0.8 for 1.4 $M_\odot$, corresponding to the condition satisfying $h_0/R_0 \leq 1/3$. Using the structure of the envelope, we have found that the color temperature differs considerably from the effective temperature, as shown in figure 3. Our conventional method needs no physical values at the hydrogen-burning shell, except for h_0.

Figure 4 shows the color temperature as a function of the distance to RX J0925.7−4758, where we have used the observed luminosity, $L = 1.6\times10^{35}(d/1\,\mathrm{kpc})^2\ \mathrm{erg\ s^{-1}}$, where d is the distance to the sources. The above luminosity and the blackbody temperature of RX J0925.7−4758 can be explained by an accreting white dwarf of mass around 1.4 $M_\odot$. The distance to the source, however, is as distant as 10 kpc or more. CAL 87, the SSS source located deep in the Large Magellanic Cloud, was also observed with ASCA. The observed spectrum was fitted with blackbody models which introduced the absorption edges as well. The derived blackbody temperature and the bolometric luminosity are 120 eV and 1.7×10^{36} erg s^{-1} for an assumed distance of 55 kpc. We cannot account for the above parameters, except for M extremely close to M_{Ch}, as inferred from figure 3.

In calculations of the color temperature we adopted the gray-atmosphere approximation, which replaces the frequency-dependent opacity, radiative flux etc. with adequate mean values. It would be necessary to solve the

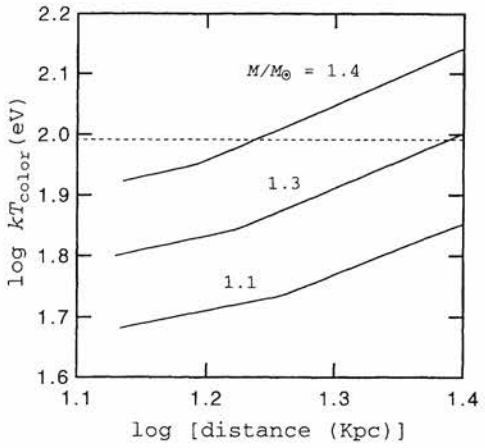

Fig. 4. Color temperature versus the distance to RX J0925.7−4758. The luminosity of this source is assumed to be $L = 1.6 \times 10^{35}(d/1\ \mathrm{kpc})^2$ erg s^{-1} (Asai et al. 1998). The broken line indicates the blackbody temperature determined from the ASCA observations.

frequency-dependent radiative transfer equation in the outer layers of the envelope to obtain a reliable spectrum. Ebisawa et al. (1997) and Asai et al. (1998) obtained the blackbody temperature and bolometric luminosity as well as the hydrogen-column density. These are strongly coupled with each other and strongly depend on the model spectra. Our calculations have revealed that the emitted spectra from the accreting white dwarf are considerably deformed from the blackbody spectra, although the deviation depends on L/L_{Edd}; a greater deviation is expected for larger L/L_{Edd}. Fitting to observations using the correct model spectra would change the bolometric luminosity and the size of the emission region remarkably; too small a size of the emission region in CAL 87 might be resolved.

One of the properties of the accreting white dwarf is the time variability in the X-ray luminosity. No quick response in the variation of the luminosity comes along with a fast variation in the accretion rate, since an increase or decrease in $\dot{M}$ exerts no immediate effect on the hydrogen-burning shell. The time scale of the variability may be given by the available nuclear energy divided by the luminosity,

$$\tau_{\mathrm{var}} = \frac{4\pi R^2 m_0 E_{\mathrm{H}}}{L} = \frac{4\pi R_0^2 m_0 E_{\mathrm{H}}}{L_{\mathrm{Edd}}} \left(\frac{L}{L_{\mathrm{Edd}}}\right)^{-1} \left(1 - \frac{M}{M_{\mathrm{Ch}}}\right), \qquad (37)$$

where m_0 is given by equation (11). For a given M, m_0 is almost constant, irrespective of L/L_{Edd}. τ_{var} is thus 1.7 for $1.1\,M_\odot$, 0.8 for $1.2\,M_\odot$, 0.3 for $1.3\,M_\odot$ and 0.08 for $1.4\,M_\odot$ in units of $(L/L_{\mathrm{Edd}})^{-1}$ years. This discriminates white dwarfs of intermediate mass at around $0.5\,M_\odot$ if time variabilities of less than one year are observed.

The stability of accreting white dwarfs with steady hydrogen-burning has been investigated by several authors (Sienkiewicz 1980 and references therein). Sienkiewicz (1980) found that the hydrogen burning shell is thermally stable for luminosities $L > 0.2L_{\mathrm{Edd}}$ for $1.39\,M_\odot$ and $L > 0.15L_{\mathrm{Edd}}$ for $0.8\,M_\odot$. According to this author, the vibrational modes are more unstable. van den Heuvel et al. (1992) modeled, using Sienkiewicz calculations, that accreting white dwarfs are unstable for $L < 0.4L_{\mathrm{Edd}}$ irrespective of the mass. If we adopt the stability condition $L > 0.4L_{\mathrm{Edd}}$, the requirement $kT_{\mathrm{color}} = 98$ eV places the source distance larger than 20 kpc. Sienkiewicz's results were, however, obtained under the method of linear analyses. Calculations of nonlinear regimes are highly anticipated.

We again emphasize that fitting to the ASCA data should be performed using realistic model spectra of accreting white dwarfs, which would provide more appropriate physical parameters that fit to accreting white dwarfs undergoing steady nuclear burning, if these are the correct models for SSSs.

We thank T. Dotani of Institute of Space and Astronautical Science for stimulated discussions on observed properties of supersoft X-ray sources.

References

Asai K., Dotani T., Nagase F., Ebisawa K., Mukai K., Smale A. 1998, in All-sky X-Ray Observation in the Next Decade, ed M. Matsuoka, N. Kawai (Seiyou Printing Co., Japan) p129

Cowley A.P., Shmidtke P.C., Crampton D., Hutching J.B. 1996, in IAU Symp. 165, Compact Stars in Binaries, ed J. van Paradijs, E.P.J. van den Heuvel, E. Kuulkers (Kluwer, Dordrecht) p439

Ebisawa K., Asai K., Mukai K., Smale A., Dotani T. 1997, in Supersoft X-Ray Sources, ed J. Greiner (Springer, Berlin) p91

Fujimoto M.Y. 1982a, ApJ 257, 752

Fujimoto M.Y. 1982b, ApJ 257, 767

Hasinger G. 1994, in the Evolution of X-Ray Binaries, ed S.S. Holt, C.S. Day, AIP Conf. Ser. 308, p611

Kahabka P. 1995, A&A 304, 227

Kahabka P., Trümper J. 1996, in IAU Symp. 165, Compact Stars in Binaries, ed J. van Paradijs, E.P.J. van den Heuvel, E. Kuulkers (Kluwer, Dordrecht) p425

Kippenhahn R., Weigert A. 1990, Stellar Structure and Evolution (Springer-Verlag, Berlin) p165

Mihalas D. 1978, Stellar Atmospheres (W.H. Freeman and Company, San Francisco) ch3

Motch C., Hasinger G., Pietsch W. 1994, A&A 284, 827

Rappaport S., Di Stefano R. 1996, in IAU Symp. 165, Compact Stars in Binaries, ed J. van Paradijs, E.P.J. van den Heuvel, E. Kuulkers (Kluwer, Dordrecht) p415
Rybicki G.B., Lightman A.P. 1979, Radiation Processes in Astrophysics (John Willy and Sons, New York) ch7
Sienkiewicz R. 1980, A&A 85, 295
Sugimoto D., Fujimoto M.Y. 1978, PASJ 30, 467
van den Heuvel E.P.J., Bhattacharya D., Nomoto K., Rappaport S.A. 1992, A&A 262, 97
Weiss A., Keady J.I., Magee N.H.Jr 1990, Atomic and Nuclear Data Tables 45, 210